symmetry

MDPI

Article

Effect of Ventricular Elasticity Due to Congenital Hydrocephalus

Hemalatha Balasundaram [1,†], Senthamilselvi Sathiamoorthy [1,†], Shyam Sundar Santra [2,*,†], Rifaqat Ali [3,†], Vediyappan Govindan [4,†], Aliona Dreglea [5,†] and Samad Noeiaghdam [5,6,†]

1 Department of Mathematics, VISTAS, Vels University, Zamin Pallavaram, Chennai 600117, Tamil Nadu, India; hemalatha.phd@velsuniv.ac.in (H.B.); senthamilselvi.sbs@velsuniv.ac.in (S.S.)
2 Department of Mathematics, JIS College of Engineering, Kalyani 741235, West Bengal, India
3 Department of Mathematics, College of Science and Arts, Muhayil, King Khalid University, Abha 9004, Saudi Arabia; rrafat@kku.edu.sa
4 Department of Mathematics, Phuket Rajabhat University, Phuket 83000, Thailand; govindoviya@gmail.com
5 Industrial Mathematics Laboratory, Baikal School of BRICS, Irkutsk National Research Technical University, 664074 Irkutsk, Russia; dreglyaai@istu.edu (A.D.); snoei@istu.edu (S.N.)
6 Department of Applied Mathematics and Programming, South Ural State University, Lenin Prospect 76, 454080 Chelyabinsk, Russia
* Correspondence: shyam01.math@gmail.com or shyamsundar.santra@jiscollege.ac.in
† These authors contributed equally to this work.

Abstract: Cerebrospinal fluid (CSF) is a symmetric flow transport that surrounds brain and central nervous system (CNS). Congenital hydrocephalusis is an asymmetric and unusual cerebrospinal fluid flow during fetal development. This dumping impact enhances the elasticity over the ventricle wall. Henceforth, compression change influences the force of brain tissues. This paper presents a mathematical model to establish the effects of ventricular elasticity through a porous channel. The current model is good enough for immediate use by a neurosurgeon. The mathematical model is likely to be a powerful tool for the better treatment of hydrocephalus and other brain biomechanics. The non-linear dimensionless governing equations are solved using a perturbation technique, and the outcome is portrayed graphically with the aid of MATLAB.

Keywords: congenital hydrocephalus; Darcy number; elasticity; fetal development; Peclet number; resistance

Citation: Balasundaram, H.; Sathiamoorthy, S.; Santra, S.S.; Ali, R.; Govindan, V.; Dreglea, A.; Noeiaghdam, S. Effect of Ventricular Elasticity Due to Congenital Hydrocephalus. *Symmetry* **2021**, *13*, 2087. https://doi.org/10.3390/sym13112087

Academic Editor: Danny Arrigo

Received: 1 October 2021
Accepted: 28 October 2021
Published: 4 November 2021

1. Introduction

Cerebrospinal fluid is an emerging fluid in biomechanics. It has been used by many researchers for prognosis of pathophysiological disorders. It has a wide interest in terms of various characteristics of flows under disparate conditions. The development of cerebrospinal fluid (CSF) is connected to the cardiovascular and respiratory systems. The heart drives blood flow, including at the beginning of CSF pulsation through the development and constriction of cerebral veins. The respiration of cardiovascular activity affects the volume of the spinal subarachnoid space (SAS). Hydrocephalus is a CSF pathology that can be analyzed to diagnose and predict the disease.

Hydrocephalus is a secretion of an excess amount of CSF in the brain parenchyma. The ventricles are enlarged with accumulated CSF due to the regular pressure of the hydrocephalus; on the other hand, the intracranial pressure remains normal. Alternatively, a large pressure gradient forms across the blockage and thus provides a mechanism responsible for ventricular expansion and tissue compression. The symptoms may vary for different age groups.

Bering et al. [1] illustrated the effects of the hydrocephalus in the absorption and origination of cerebrospinal fluid within the cerebral ventricles. An experiment has been conducted using dog CSF to determine the resistance and pressure of the fluid flow followed by injecting a drug into the ventricular volume through various experiments.

Pressure differences between SAS and lateral ventricles and differences between the observed and predicted CSF pulsatile flow velocities in the anterior area point towards brain was shown by Lininger et al. [2].

The distribution of any drug in the brain, such as interleukin-2, is controlled by the transport route contained in the brain and on the various drug effects, such as concentration, hydrophobicity, and corresponding brain tissue, as was illustrated in S. Kalyanasundaram et al. [3]. The model shows the intracranial pressure (ICP) in a pulsatile motion, which results in the changes in cerebral blood volume that occur within a rigid space. At minimum and moderate values of ICP, the amplitude mainly reflects the cerebral pressure-volume, as studied by Mauro Ursino [4].

Minor pathway hydrocephalus based on the progression of CSF dynamics was simulated by Nigel Peter Syms et al. [5]. A three-dimensional fluid construction connection displaying was used for recreation of contrasted and ordinary non-communicating hydrocephalus (NCH) patients at the pre-treatment stage. Assessment of ventricles' volume and increase in CSF pressure (prior to shunting) following outcome approval showed that these boundaries were the most legitimate hydrodynamic lists and that the NCH type does not have any critical impact on changes, as clearly illustrated in Seifollah Gholampour [6]. The pressure volume model for a CSF hydrocephalus to predict the nature of ventricle flow pressure and its excretion volume was developed by Kauffman J and Drapaca [7].

A case report on treatment under intracranial pressure observation with a bilateral ventriculoperitoneal switch for negative pressure hydrocephalus was clearly estimated by Sajan Pandey et al. [8]. The instinctive bearings of brain analysis using the various known methods of mechanics were discussed by Karol Miller et al. [9]. Three-dimensional computational models of the cerebrospinal fluid (CSF) stream and cerebrum tissue are introduced for the assessment of their hydrodynamic conditions prior to and then after shunting for seven patients with non-imparting hydrocephalus, as described by S. Gholampour et al. [10]. Keith Sharp et al. [11] described a model to express the significance of Taylor dispersion in thesSuperior subarachnoid space (SSS), and "glymphatic system" spaces might be controlled clinically for the improvement of fluid transportation.

The computational model portrays the pulsatile twisting of the third ventricle due to the beating of blood vessels and the subsequent CSF elements inside cerebrum pathways. This demonstrates that the lateral ventricles' development prompts an unloading impact on the strain applied to the dividers of the ventricles. These outcomes may lead to minimized intracranial strain (ICP) adequacy, as studied by João Apura et al. [12]. CSF imaging advances that provide a better idea of CSF dynamics and the pathophysiology of hydrocephalus with an pulse image of CSF dynamics were shown in Shinya Yamada et al. [13]. A computational study analyzed the effects on the flow and elastic behavior over the ventricle walls. Differences of the results are processed by clinical data solved with the Time-SLIP MRI, which entrap ventricular CSF flows for affected patients, as investigated by Willlam W. Liou et al. [14] and G Soza et al. [15].

A multi-phase poro-elastic model for the mind is important, depending on clinical information. The model can be utilized to portray the solid brain, the cerebrum with hydrocephalus, and the progress between them because of an adjustment of model boundaries was illustrated by G. S. Yan'kova et al. [16]. The numerical method based on Blasius's approach for flow past a flat plate in the case of heat transfer for large Reynolds numbers has been discussed by Dreglea and Shishkin [17] and also in [18]. There are two models, namely development and normophysiology, and hypoxic and hypercapnic conditions. These models process the physiological variables identified especially in adult humans under both pathological conditions and in normal conditions, which explain the basic mechanisms analysed by Antonio Albanese et al. [19]. Inlet and outlet boundary conditions used to improve the computational simulation of hydrocephalus patients were modeled by Seifollah Gholampour & Nasser Fatouraee [20]. Pathophysiology of hydrocephalus its different types are clearly explained by Deepak Gupta et al. [21], and a bio-mechanical model of the brain was studied in a book authored by K. Miller et al. [22].

Hydrocephalus in porous media has been illustrated by B. Hemalatha and S. Senthamilselvi [23].

Elasticity plays a major role in congenital hydrocephalus, which implies the ventricle shape. The most well-known treatment for hydrocephalus is the careful inclusion of a drainage system called a shunt, which is an adaptable cylinder with a valve that keeps liquid from the cerebrum streaming the correct way and at the appropriate rate. Every month, the CSF secretion in a human body will be approximately 400–600 (depends on age). As the CSF acts as a mass transfer, it will secreted and absorbed blood around three time per day.

In this paper, we develop a mathematical model for unsteady and asymmetric viscous incompressible fluid flow for porous parenchyma due to congenital hydrocephalus. To the best of the authors' knowledge, the effect of elasticity with a chemical reaction on the hydrocephalus's asymmetric channel has not been studied in the literature. The purpose of this paper is to analyze the lateral ventricular elasticity for congenital hydrocephalus in an asymmetric flow with species concentration. The governing equations of fluid flow are solved subject to relevant boundary conditions. The influence of various parameters on velocity, "u", and species concentration, "c", is studied, and analytical results obtained are shown graphically. The problem is characterized in Section 2, and Section 3 incorporates the solutions for flow and mass transport analysis. The graphical results are presented and discussed in Section 4. Section 5 contains the summary and conclusions.

2. Mathematical Formulation

CSF is a water-like viscous incompressible Newtonian fluid [3]. CSF can be considered as an unsteady laminar flow bounded by porous parenchyma pia matter and Dura matter [11]. CSF is produced by ventricles of choroid plexus more adequate in the first two lateral ventricles, providing nutrients that remove waste diffusions, and helps to protect the brain from skull damage. Later, CSF will be absorbed by arachnoid granulation called Arachnoid villi. The barrier between the CSF and the blood in these granulations is thin, enabling CSF to pass into the bloodstream, where it is absorbed and passes throughout the body as a blood.

Congenital hydrocephalus is an abnormal free-convection CSF flow that deforms the ventricular size. We have discussed the flow shunt by hydrocephalus in which the fluid flows through porous media. Here, lateral ventricles act as a viscoelastic model. We extended the paper of B. Hemalatha and S. Senthamilselvi [23] to describe the effects of hydrocephalus in porous media with elasticity. Viscous and Darcy's resistance terms are considered with constant permeability of the porous medium. Let us take the cartesian coordinates as x and y in which the fluid flows are normal to one another. C refers to the species concentrations at the walls with mass diffusion coefficient D. Under these assumptions, the governing equations for CSF in an asymmetric channel with resistance was incorporated in Figure 1 may be written as:

$$\frac{\partial \tilde{v}}{\partial \tilde{y}} = 0. \tag{1}$$

Let us consider the Navier–Stokes Equation of [11] Hemalatha et al., with elasticity as

$$\frac{\partial \tilde{u}}{\partial \tilde{t}} + Gv_0 \frac{\partial \tilde{u}}{\partial \tilde{y}} = \frac{-1}{\rho} \frac{\partial \tilde{p}}{\partial \tilde{x}} + \nu \frac{\partial^2 \tilde{u}}{\partial \tilde{y}^2} + \frac{RN}{\rho} \tilde{u} + \frac{\nu}{k} \tilde{u}. \tag{2}$$

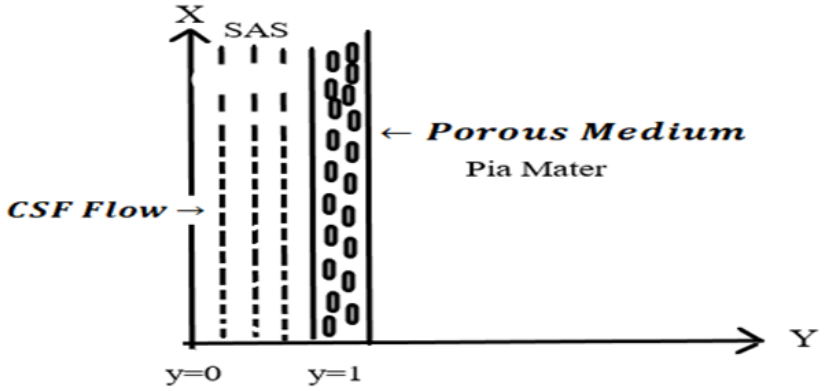

Figure 1. Fluid flow configuration.

The following equation represents the molecular diffusivity of cerebrospinal fluid

$$\frac{\partial \tilde{c}}{\partial \tilde{t}} + v_0 \frac{\partial \tilde{c}}{\partial \tilde{y}} = D \frac{\partial^2 \tilde{c}}{\partial \tilde{y}^2} - k\tilde{c} \tag{3}$$

with suitable boundary conditions,

$$if\ \tilde{y} = 0,\ \ then\ \tilde{u} = 0,\ \tilde{c} = 1;$$

$$if\ \tilde{y} = h,\ \ then\ \tilde{u} = 1,\ \tilde{c} = 0.$$

Here,˜ indicates the parameters with different dimensions and units. After the equations are non-dimensionalized, the governing equations from (1) to (3) will become

$$\frac{\partial v}{\partial y} = 0, \tag{4}$$

$$Re\left[\frac{\partial u}{\partial t} + G\frac{\partial u}{\partial y}\right] = -\frac{\partial P}{\partial x} + \nu \frac{\partial^2 u}{\partial y^2} + G_p u + S^2 u, \tag{5}$$

$$\frac{\partial c}{\partial t} + \frac{\partial c}{\partial y} = \frac{1}{Pe}\frac{\partial^2 c}{\partial y^2} - kc, \tag{6}$$

with the corresponding boundary conditions,

$$if\ y = 0,\ \ then\ \tilde{u} = 0,\ \tilde{c} = 1;$$

$$if\ y = 1,\ \ then\ \tilde{u} = 1,\ \tilde{c} = 0.$$

In the non-dimensional governing equations, the following dimensionless quantities are introduced:

$$u = \frac{\tilde{u}}{v_0}; P = \frac{\tilde{p}}{\rho v_0 \nu}; t = \frac{v_0 \tilde{t}}{h}; y = \frac{\tilde{y}}{h};$$

$$x = \frac{\tilde{x}}{h}; G = \frac{stress}{strain}(Young's\ modulus); c = \frac{\tilde{c}}{c_0}$$

$$G_p = \frac{Rh^2 N}{\nu \rho}(Particle\ mass\ parameter); Da = \frac{K}{h^2}(Darcy\ number);$$

$$Re = \frac{h v_0}{\nu}(Reynolds\ Number); Pe = \frac{v_0 h}{D}(Peclet\ number);$$

$$S = \frac{1}{Da}; K = \frac{hk}{v_0}(Reciprocal\ of\ Darcy\ number); K = \frac{hk}{v_0}(Chemical\ reaction\ parameter).$$

3. Method of Solution

The non-linear partial differential Equations (4)–(6) are quite challenging to solve using an analytical method; therefore, we put forth a perturbation technique to solve the non-linear PDE. We represent an arbitrary constant perturbation parameter $\epsilon(\epsilon << 1)$ for the fluid velocity, pressure, and transport diffusivity term using the support of various parameters such as the Reynolds number, resistance parameter, Youngs modulus, Peclet number for mass transfer, and the permeability parameter Darcy number.

Let us consider velocity U, pressure P, and concentration C as follows,

$$U(y,t) = u^0 + \epsilon e^{\lambda t} u^1 + O(\epsilon^2), \tag{7}$$

$$P(y,t) = u + \epsilon e^{\lambda t} p^1 + O(\epsilon^2), \tag{8}$$

$$C(y,t) = c^0 + \epsilon e^{\lambda t} c^1 + O(\epsilon^2), \tag{9}$$

omitting the higher order of $O(\epsilon^2)$. Using Equations (7)–(9) in (5) and (6), we get

$$\frac{d^2u^0}{dy^2} - GRe\frac{du^0}{dy} + (G_p + S^2)u^0 = g, \tag{10}$$

$$\frac{d^2u^1}{dy^2} - GRe\frac{du^1}{dy} - (\lambda Re - G_p - S^2)u^1 = 0, \tag{11}$$

$$\frac{d^2c^0}{dy^2} - Pe\frac{dc^0}{dy} - KPe\, c^0 = 0, \tag{12}$$

$$\frac{d^2c^1}{dy^2} - Pe\frac{dc^1}{dy} - Pe(\lambda + k)c^1 = 0. \tag{13}$$

The base u^0, c^0 and perturbed part u^1, c^1 of the momentum and transport diffusivity equation are given by

$$u^0 = A_{01}e^{m_1 y} + A_{02}e^{m_2 y} + \frac{p}{Gp + S^2}, \tag{14}$$

$$u^1 = A_{13}e^{m_3 y} + A_{14}e^{m_4 y}, \tag{15}$$

$$c^0 = B_{01}e^{m_5 y} + B_{02}e^{m_6 y}, \tag{16}$$

$$c^1 = B_{17}e^{m_7 y} + B_{18}e^{m_8 y}. \tag{17}$$

The value of the constants in base and perturb part were clearly illustrated in Appendix A.

Using the perturbation technique, the equations of momentum and species concentration are assumed as,

$$U(x,y,t) = u^0 + \epsilon e^{\lambda t} u^1,$$
$$C(x,y,t) = c^0 + \epsilon e^{\lambda t} c^1.$$

Substituting the above Equations (14)–(17) in the above result, we get,

$$U(x,y,t) = A_{01}e^{m_1 y} + A_{02}e^{m_2 y}\frac{p}{Gp + S^2} + \epsilon e^{\lambda t}(A_{13}e^{m_3 y} + A_{14}e^{m_4 y}), \tag{18}$$

$$C(x,y,t) = B_{01}e^{m_5 y} + B_{02}e^{m_6 y} + \epsilon e^{\lambda t}(B_{17}e^{m_7 y} + B_{18}e^{m_8 y}). \tag{19}$$

4. Results and Discussion

The analytical solution of the present problem is determined using the perturbation technique, and the results are portrayed in graph, showing the interesting features and significance of the physical parameters on velocity and concentration. To study the effects of elasticity of congenital hydrocephalus in an asymmetric flow channel, the velocity u and the species concentration profiles C are depicted graphically against y for different values

of different parameters such as the particle mass parameter, Darcy number S^2, Young's modulus G, Reynolds number Re, Peclet number for mass transfer, and chemical reaction parameter K. The graphs were plotted using MATLAB. As the Reynolds number varies from 150 to 420, we have estimated the error and it has been disported in Table 1.

The Reynolds number of the fluid flow ranges from 150 to 420. The inertial force increases predominantly as the CSF drains the entire ventricles. In Figure 2, the Reynolds number significantly increases as the ventricle size increases, after which the fluid gets drained by lumbar puncture through suction. Hence, the excess fluid passes to the digestive system.

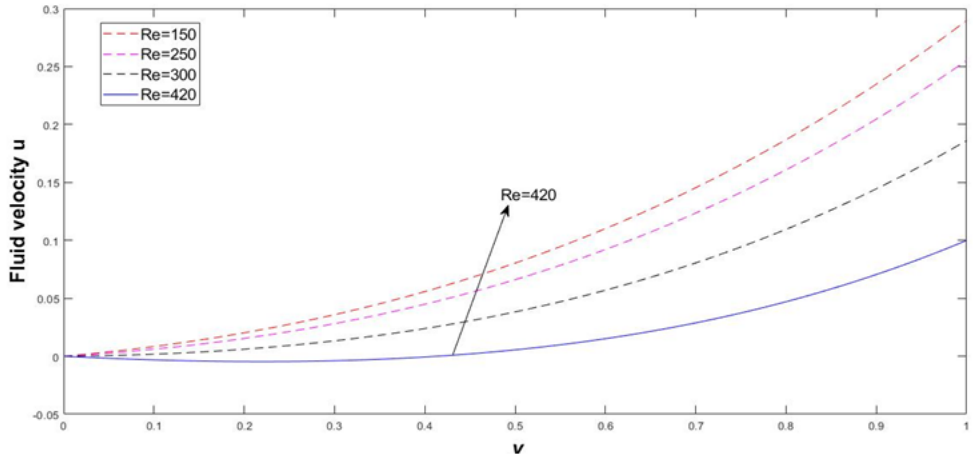

Figure 2. Variation of Reynolds number 'Re' in velocity distribution with $t = 0.1, G = 0.901, \lambda = 0.3, g = 0.37, \epsilon = 0.01, Gp = 0.33$.

In Figure 3, there is a lesser resistance after the fluid level increases and then Gp slowly rises. Henceforth, it can be biologically interpreted that the lateral ventricle deforms back to its original spot.

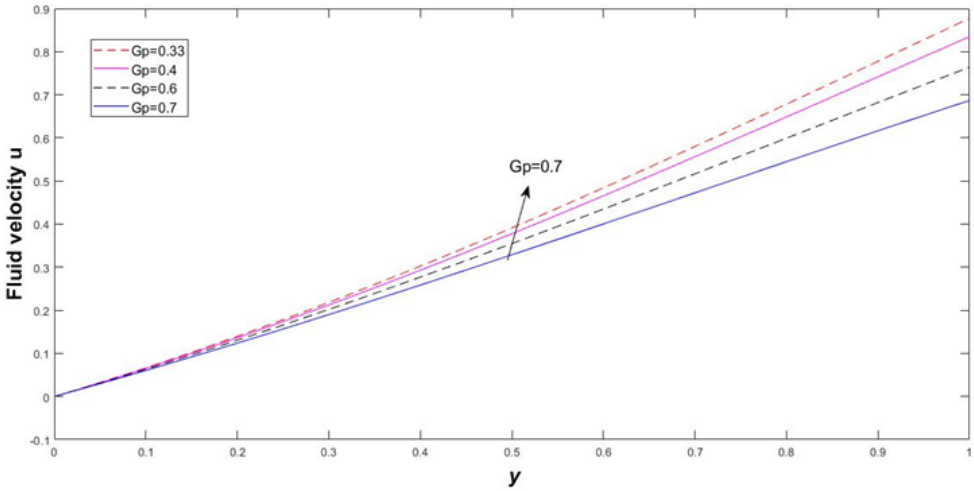

Figure 3. Variation of particle mass parameter 'Gp' in velocity distribution with $t = 0.1, G = 0.901, g = 0.37, \lambda = 0.3, \epsilon = 0.01, Gp = 0.33, Re = 150$.

There is a significant increase in pressure difference and Young's modulus of elasticity, and rate of deformation with strain (G) increases due to congenital hydrocephalus in Figure 4. It is understood clearly that the rate of deformation increases with the increase in fluid velocity.

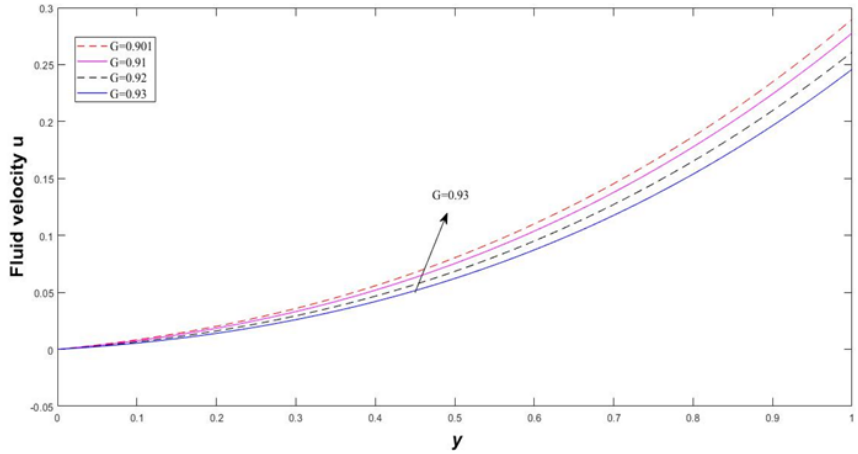

Figure 4. Variation of Youngs Modulus G in velocity distribution with $t = 0.1, \lambda = 0.3, \epsilon = 0.01, g = 0.37, Re = 150, Gp = 0.3, Da = 0.33$.

The permeability of the fluid medium increases as it retains its elasticity with respect to its characteristic length of layer considered in Figure 5. The Darcy number is assumed not to exceed 1, and it increases as velocity of the fluid increases.

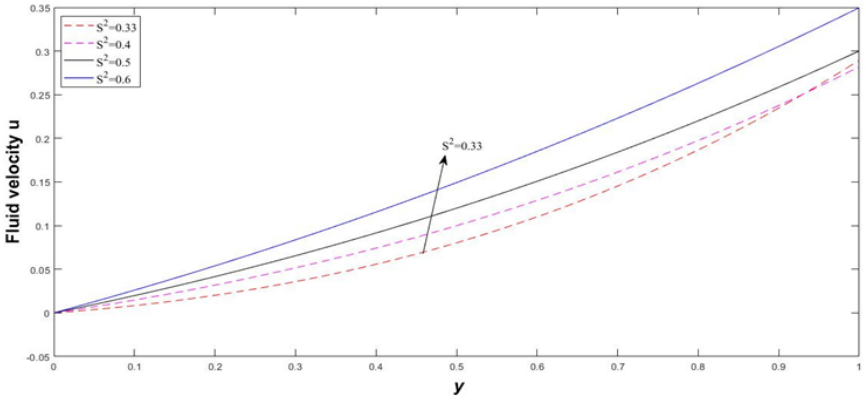

Figure 5. Variation of Darcy number Da in velocity distribution with $t = 0.1, \lambda = 0.3, \epsilon = 0.01, p = 0.37, Re = 150, Gp = 0.3, G = 0.901$.

The mass transfer parameter increases advection transport rate in a promising way compared to the diffusive transport. There is an adequate motion of fluid due to the nature of the hydrocephalus. Hence, it is understood that the chemical reaction increases as the fluid transport diffusivity decreases has given in Figure 6.

To understand the characteristic behavior of the velocity and concentration, fluid flow (v) and (c) are calculated by varying the emerging flow parameters such as Young's Modulus, particle mass parameter, Reynolds Number, Darcy Number, and Peclet Number. The obtained results are influenced graphically to show the different values of various parameters. We calculated the statistical error as the Reynolds number increases from 150 to 420 to achieve the error approximation.

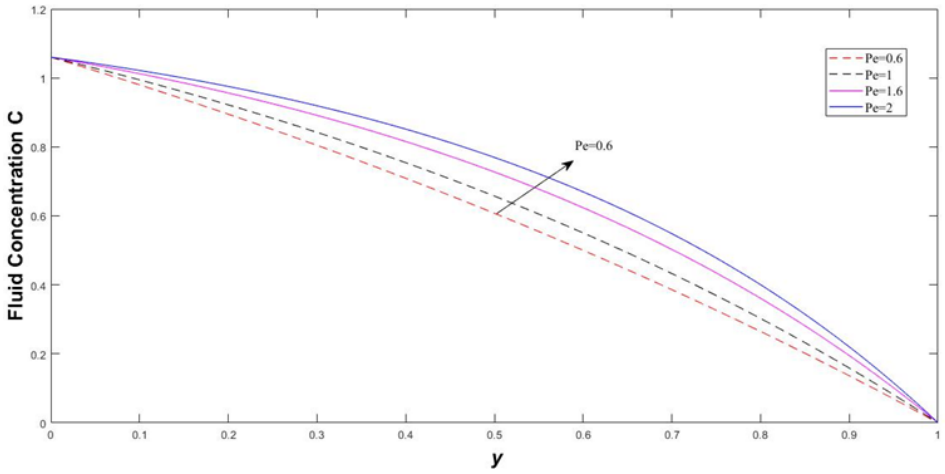

Figure 6. Variation of Peclet number 'Pe' in concentration distribution with $k = 0.03, t = 0.1, \epsilon = 0.06$, and $\lambda = 0.03$.

Error Approximation for Dimensionless Number (Re)

Percentage of error for the flow velocity for Reynolds number from 150 to 340 by using the truncation error is given in Table 1.

Table 1. Error Estimation for Reynolds Number.

Re	Velocity of Fluid Flow		Relative Error	|Error| %
	True Value	Measured Value		
150	-4.19×10^{134}	1.4536×10^{135}	−0.776109002	77.61090023
250	-1.87×10^{135}	6.4925×10^{135}	−0.776109002	77.61090023
317	-8.37×10^{135}	2.8998×10^{136}	−0.776109002	77.61090023
322	-3.74×10^{136}	1.2952×10^{137}	−0.776109002	77.61090023
340	-1.67×10^{137}	-1.6688×10^{137}	−0.776109002	77.61090023

5. Conclusions

The present study highlights the comprehension of CSF dynamics in the population affected by hydrocephalus. Further, the upgraded biocompatible material and novel strategies are recommended to be utilized in the creation of models to limit the danger of avoidable diseases. Continuous study assists with deciding seriousness of sickness and increasing the doctor's understanding during clinical evaluation and anticipation of patients' conditions. The development of CSF during constrained convection can be distinguished at the level of the brain during hydrocephalus. Reynolds Re and Peclet Number Pe increases significantly with fluid velocity and concentration in the region.

The effect of increasing Elastic (Young's) modulus parameter increased eventually as the rates of velocity distributions are enhanced. The effect of velocity distribution is increased rapidly with increasing Reynolds number. The rate of velocity profile in the form of a graph is increased with increasing porosity parameter. The concentration of the fluid layer is enhanced with rises in the Peclet number. The momentum of the cerebrospinal fluid increases corresponding to the various resistance parameters and porosity parameter, the Darcy number.

It can be concluded that the establishment of CSF resistance and elasticity are not adequate to explain the mechanism of ventricular hump and depletion. Therefore, cardinal studies are needed on the tissue-related effects of brain parenchyma, dura and cranium; their relationship to cerebrospinal parameters; and how both are altered by the hydrocephalic process. Finally, we conclude that our study, along with the neurological literature, shows that that an active part of the brain elasticity in the etiology of adult hydrocephalusto can help professionals to identify the statistical findings for various patients.

Author Contributions: Conceptualization, H.B., S.S., S.S.S., R.A., V.G., A.D. and S.N.; methodology, H.B., S.S., S.S.S., R.A., V.G., A.D. and S.N.; software, H.B., S.S., S.S.S., R.A., V.G., A.D. and S.N.; validation, H.B., S.S., S.S.S., R.A., V.G., A.D. and S.N.; formal analysis, H.B., S.S., S.S.S., R.A., V.G., A.D. and S.N.; investigation, H.B., S.S., S.S.S., R.A., V.G., A.D. and S.N.; resources, H.B., S.S., S.S.S., R.A., V.G., A.D. and S.N.; data curation, H.B., S.S., S.S.S., R.A., V.G., A.D. and S.N.; writing—original draft preparation, H.B., S.S., S.S.S., R.A., V.G., A.D. and S.N.; writing—review and editing, H.B., S.S., S.S.S., R.A., V.G., A.D. and S.N.; visualization, H.B., S.S., S.S.S., R.A., V.G., A.D. and S.N.; supervision, H.B., S.S., S.S.S., R.A., V.G., A.D. and S.N.; project administration, H.B., S.S., S.S.S., R.A., V.G., A.D. and S.N.; funding acquisition, R.A., A.D. and S.N. All authors have read and agreed to the published version of the manuscript.

Funding: This research was funded by Deanship of Scientific Research at King Khalid University grant number R.G.P2/39/42.

Acknowledgments: We are very grateful to the editor and unbiased arbitrator for their prudent interpretation and proposition, which refined the excellency of this manuscript. The authors extend their appreciation to the Deanship of Scientific Research at King Khalid University for funding through a research group program under grant number R.G.P2/39/42.

Conflicts of Interest: The authors declare no conflict of interest.

Nomenclature

CSF	cerebrospinal fluid
$\tilde{x}, \tilde{y}$	cartesian coordinates
x, y	dimensionless cartesian coordinates
$\tilde{t}$	time parameter
t	dimensionless time parameter
$\tilde{c}$	concentration of the fluid
c	dimensionless concentraion
SAS	subarachnoid space
$\tilde{p}$	fluid pressure
$\tilde{u}, \tilde{v}$	velocity of the fluid flow
u, v	dimensionless velocity of the fluid flow
h	characteristics length
u_0	initial velocity of the fluid flow
λ	positive real constant
c_0	initial concentration of the fluid
u, v	Velocity of the fluid
ν	Kinematic viscosity of the fluid
ρ	Density of the fluid
G	(elasticity) Young's modulus of the fluid flow
p	dimensionless constant pressure
K	chemical reaction parameter
g	dimensionless pressure
k	Permeability of the porous medium
D	Coefficient of mass diffusivity of the fluid
Pe	Peclet number for mass transfer
Re	Reynolds Number
Da	Darcy Number
Gp	particle mass parameter
ϵ	perturbation parameter ($\epsilon \ll 1$)

Appendix A

$$
\begin{aligned}
m_1 &= \frac{GRe + \sqrt{(GRe)^2 - 4(Gp + S^2)}}{2} \\
m_2 &= \frac{GRe - \sqrt{(GRe)^2 - 4(Gp + S^2)}}{2} \\
A_{01} &= -A_{02} - \frac{p}{Gp + S^2} \\
A_{02} &= \frac{1}{e^{m_2} - 1}\left[1 - \frac{p(e^{m_1} - 1)}{Gp + S^2}\right] \\
m_3 &= \frac{GRe + \sqrt{(GRe)^2 - 4(\lambda Re - Gp - S^2)}}{2} \\
m_4 &= \frac{GRe - \sqrt{(GRe)^2 - 4(\lambda Re - Gp - S^2)}}{2} \\
A_{13} &= -A_{14} \\
A_{14} &= \frac{1}{e^{m_4} - e^{m_3}} \\
m_5 &= \frac{Pe + \sqrt{(Pe)^2 + 4(KPe)}}{2} \\
m_6 &= \frac{Pe - \sqrt{(Pe)^2 + 4(KPe)}}{2} \\
B_{01} &= -B_{02} \\
B_{02} &= \frac{-e^{m_5}}{e^{m_6} - e^{m_5}} \\
m_7 &= \frac{Pe + \sqrt{(Pe)^2 + 4Pe(K + \lambda)}}{2} \\
m_8 &= \frac{Pe - \sqrt{(Pe)^2 + 4Pe(K + \lambda)}}{2} \\
B_{17} &= -B_{18} \\
B_{18} &= \frac{-e^{m_7}}{e^{m_8} - e^{m_7}}.
\end{aligned}
$$

Here we used MATLAB coding to portrait the graphical form of the above analytical method.

Hence determine the momentum equation and transport diffusivity equation we use the following MATLAB coding to predict the nature of cerebrospinal fluid flow velocity and its concentration.

```
%%%%%%%%%%%%%%%%%% Momentum Equation %%%%%%%%%%%
m1 = (1/2) * (Re * G + sqrt((Re * G)^2 - (4 * (Gp - s^2))));
m2 = (1/2) * (Re * G - sqrt((Re * G)^2 - (4 * (Gp - s^2))));
A02 = (1/(exp(m2)) - 1) * (1 - (p * (1 - exp(m1))/(Gp - (s^2))));
A01 = -A02 - (p/Gp - s^2);
u0 = (A01 * exp(m1 * y)) + (A02 * exp(m2 * y)) + (p/Gp - s^2);
m3 = (1/2) * (Re * G + sqrt((Re * G)^2 + (4 * (Re * lambda) - Gp + s^2)));
m4 = (1/2) * (Re * G - sqrt((Re * G)^2 + (4 * (Re * lambda) - Gp + s^2)));
u1 = (exp(m4 * y) - exp(m3 * y))/(exp(m4) - exp(m3));
u = (u0) + ((epsilon * exp(lambda * t)) * (u1));
plot(y, u,' m-',' Linewidth', 1);hold on
%%%%%%%%%%%%% % Concentration Equation % %%%%%%%%
a1 = sqrt((pe)^2 + (4 * k * pe));
m5 = (pe + a1)/2;
```

$$
\begin{aligned}
&m6 = (pe - a1)/2;\\
&a2 = m5 * y;\\
&a3 = m6 * y;\\
&a4 = exp(a3) - exp(a2);\\
&c0 = exp(a2) - (exp(m5) * (a4)/(exp(m6) - exp(m5)));\\
&b1 = sqrt((pe)^2 + (4 * (k + lambda) * pe));\\
&m7 = (pe + b1)/2;\\
&m8 = (pe - b1)/2;\\
&b2 = m7 * y;\\
&b3 = m8 * y;\\
&b4 = exp(b3) - exp(b2);\\
&c1 = exp(b2) - (exp(m7) * (b4)/(exp(m8) - exp(m7)));\\
&c = (c0) + ((epsilon * exp(lambda * t)) * (c1));\\
&plot(y, c, 'm-', 'Linewidth', 1);\text{hold on}\\
&\%\%\%\%\%\%\%\%\%\ \%\%\%\%\%\%\%\%\%\ \%\%\%\%\%\%\%\%\%
\end{aligned}
$$

References

1. Bering, E.A.; Sato, O. Hydrocephalus: Changes in Formation and Absorption of Cerebrospinal Fluid Within the Cerebral Ventricles. *J. Neurosurg.* **1963**, *20*, 1050–1063. [CrossRef] [PubMed]
2. Linninger, A.A.; Xenos, M.; Zhu, D.C.; Somayaji, M.R.; Kondapalli, S.; Penn, R.D. Cerebrospinal Fluid Flow in the Normal and Hydrocephalic Human Brain. *IEEE Trans. Biomed. Eng.* **2007**, *54*, 291–302. [CrossRef] [PubMed]
3. Kalyanasundaram, S.; Calhoun, V.D.; Leong, K.W. A finite element model for predicting the distribution of drugs delivered intracranially to the brain. *Am. J. Physiol. Integr. Comp. Physiol.* **1997**, *273*, R1810–R1821. [CrossRef] [PubMed]
4. Ursino, M. A mathematical study of human intracranial hydrodynamics part 1—The cerebrospinal fluid pulse pressure. *Ann. Biomed. Eng.* **1988**, *16*, 379–401. [CrossRef] [PubMed]
5. Symss, N.P.; Oi, S. Theories of cerebrospinal fluid dynamics and hydrocephalus: historical trend. *J. Neurosurg. Pediatr.* **2013**, *11*, 170–177. [CrossRef] [PubMed]
6. Gholampour, S. FSI simulation of CSF hydrodynamic changes in a large population of non-communicating hydrocephalus patients during treatment process with regard to their clinical symptoms. *PLoS ONE* **2018**, *13*, e0196216. [CrossRef] [PubMed]
7. Kauffman, J.; Drapaca, C.S. A Fractional Pressure-Volume Model of Cerebrospinal Fluid Dynamics in Hydrocephalus. In *Mechanics of Biological Systems and Materials*; Barthelat, F., Zavattieri, P., Korach, C., Prorok, B., Grande-Allen, K., Eds.; Springer: Cham, Switzerland, 2014; Volume 4. [CrossRef]
8. Pandey, S.; Jin, Y.; Gao, L.; Zhou, C.C.; Cui, D.M. Negative-Pressure Hydrocephalus: A Case Report on Successful Treatment Under Intracranial Pressure Monitoring with Bilateral Ventriculoperitoneal Shunts. *World Neurosurg.* **2017**, *99*, 812.e7–812.e12. [CrossRef] [PubMed]
9. Miller, K.; Wittek, A.; Tavner, A.C.R.; Joldes, G.R. Biomechanical Modelling of the Brain for Neurosurgical Simulation and Neuroimage Registration. In *Biomechanics of the Brain. Biological and Medical Physics, Biomedical Engineering*; Miller, K., Ed.; Springer: Cham, Switzerland, 2019. [CrossRef]
10. Gholampour, S.; Fatouraee, N.; Seddighi, A.S. Numerical simulation of cerebrospinal fluid hydrodynamics in the healing process of hydrocephalus patients. *J. Appl. Mech. Tech. Phys.* **2017**, *58*, 386–391. [CrossRef]
11. Sharp, M.K.; Carare, R.O.; Martin, B.A. Dispersion in porous media in oscillatory flow between flat plates: applications to intrathecal, periarterial and paraarterial solute transport in the central nervous system. *Fluids Barriers CNS* **2019**, *16*, 13. [CrossRef]
12. Apura, J.; Tiago, J.; Moura, A.; Lourenço, J.A.; Sequeira, A. The effect of ventricular volume increase in the amplitude of intracranial pressure. *Comput. Methods Biomech. Biomed. Eng.* **2019**, *22*, 889–900. [CrossRef]
13. Yamada, S.; Kelly, E. Cerebrospinal Fluid Dynamics and the Pathophysiology of Hydrocephalus: New Concepts. *Semin. Ultrasound CT MRI* **2016**, *37*, 84–91. [CrossRef] [PubMed]
14. Liou, W.W.; Yang, Y.; Yamada, S. Cerebrospinal Fluid Flow Simulations in Brain Ventricles With Elastic Wall Responses. In Proceedings of the 6th International Conference on Computational and Mathematical Biomedical Engineering—CMBE2019, Sendai City, Japan, 10–12 June 2019.
15. Soza, G.; Grosso, R.; Nimsky, C.; Hastreiter, P.; Fahlbusch, R.; Greiner, G. Determination of the elasticity parameters of brain tissue with combined simulation and registration. *Int. J. Med. Robot. Comput. Assist. Surg.* **2005**, *1*, *87*. [CrossRef]
16. Yan'kova, G.S.; Cherevko, A.A.; Khe, A.K.; Bogomyakova, O.B.; Tulupov, A.A. Study of Hydrocephalus Using Poroelastic Models. *J. Appl. Mech. Tech. Phys.* **2020**, *61*, 14–24. [CrossRef]
17. Dreglea, A.I.; Shishskin, G.I. Robust numerical method based on Blasius approach for flow past a flat plate in the case of heat transfer for large Reynolds numbers. In Proceedings of the CMAM-1, Minsk, Belarus, 21–25 July 2003; pp. 19–20.

18. Dreglea, A.I.; Shishskin, G.I. Numerical method based on Blasius approach for flow past flat plate in the case of heat transfer for large Reinolds numbers. In Proceedings of the Annual Symposium of Irish Society for Scientific and Engineering Computation, Belfield, Dublin, Ireland, 23–24 May 2003; p. 14.
19. Albanese, A.; Cheng, L.; Ursino, M.; Chbat, N.W. An integrated mathematical model of the human cardiopulmonary system: model development. *Am. J. Physiol. Circ. Physiol.* **2016**, *310*, H899–H921. [CrossRef] [PubMed]
20. Gholampour, S.; Fatouraee, N. Boundary conditions investigation to improve computer simulation of cerebrospinal fluid dynamics in hydrocephalus patients. *Commun. Biol.* **2021**, *4*, 394. [CrossRef] [PubMed]
21. Gupta, D.; Singla, R.; Dash, C. Pathophysiology of Hydrocephalus. In *Hydrocephalus*; Ammar A., Ed.; Springer: Cham, Switzerland, 2017. [CrossRef]
22. Miller, K. (Ed.) *Biomechanics of the Brain*; Biological and Medical Physics, Biomedical Engineering; Springer: Cham, Switzerland, 2019. [CrossRef]
23. Hemalatha, B.; Senthamil, S. Effect of Cerebrospinal Fluid Dynamics with Hydrocephalus in Porous Medium. *Turk. J. Comput. Math. Educ.* **2021**, *12*, 5666–5671.